

Article

Phosphate Uptake by Precipitation in Model Animal Wastewaters: Adjusting Ionic Strength and Ionic Composition to Maximize Phosphorus Removal

Elizabeth C. Butler ^{*}, Yifan Ding  and David A. Sabatini

School of Civil Engineering and Environmental Science, University of Oklahoma, Norman, OK 73019-1024, USA; yfding@ou.edu (Y.D.); sabatini@ou.edu (D.A.S.)

^{*} Correspondence: ecbutler@ou.edu

Abstract: While phosphorus is a limited resource that is essential for agriculture, its release to the environment adversely impacts water quality. At the same time, animal wastewaters contain significant quantities of phosphorus and nitrogen that can be recovered for beneficial use. Phosphorus uptake experiments were performed with magnesium-treated corn-cob char and with magnesium silicate prepared using silicate from rice straw at pH 8 and 9. The concentration of dissolved phosphorus as a function of total added ammonium chloride (NH_4Cl) was determined, and chemical equilibrium modeling was used to investigate the concentration trends of dissolved and mineral species. According to chemical equilibrium modeling, carbonate alkalinity exerted a significant magnesium demand, with approximately half of all added magnesium forming magnesite ($\text{MgCO}_3(\text{s})$). As total added NH_4Cl increased, excess Cl^- complexed with dissolved Mg^{2+} in competition with orthophosphate, freeing orthophosphate to precipitate, mainly as the mineral struvite ($\text{NH}_4\text{MgPO}_4 \cdot 6\text{H}_2\text{O}(\text{s})$). As the concentration of added NH_4Cl increased by a factor of ten, measured concentrations of dissolved phosphorus decreased by a factor of ten, meaning that ionic composition has the potential to significantly impact the amount of phosphorus that can be recovered from wastewaters for beneficial use.



Citation: Butler, E.C.; Ding, Y.; Sabatini, D.A. Phosphate Uptake by Precipitation in Model Animal Wastewaters: Adjusting Ionic Strength and Ionic Composition to Maximize Phosphorus Removal. *Water* **2022**, *14*, 2229. <https://doi.org/10.3390/w14142229>

Academic Editors: Charalambos Papelis

Received: 24 June 2022

Accepted: 14 July 2022

Published: 15 July 2022

Publisher's Note: MDPI stays neutral with regard to jurisdictional claims in published maps and institutional affiliations.



Copyright: © 2022 by the authors. Licensee MDPI, Basel, Switzerland. This article is an open access article distributed under the terms and conditions of the Creative Commons Attribution (CC BY) license (<https://creativecommons.org/licenses/by/4.0/>).

Keywords: phosphorus recovery; fertilizer; eutrophication; struvite; bobierrite; animal wastewater; biochar

1. Introduction

While phosphorus is essential for food production, global reserves of concentrated phosphorus minerals are limited, and expected population growth will require increased food production, and thus, increased phosphorus fertilizer, to meet world food needs. In addition, releases of dilute phosphorus wastes to natural waters are responsible for eutrophication and its impacts on water quality and fisheries, tourism, and other coastal activities, with a total global annual economic impact estimated in the tens of billions of dollars [1]. Consequently, efficient waste treatment for phosphorus recovery and reuse is needed to achieve sustainable phosphorus use and promote water quality.

One major source of phosphorus is wastewaters from animal production facilities. Two billion tons of solid wastes from animal production are generated annually in the United States—nine times the amount from American homes [2]—which is an enormous source of phosphorus that can be recovered for beneficial use. Most large U.S. livestock facilities treat manure in open or covered anaerobic lagoons and digesters that destroy organic matter and remove some nitrogen by volatilization, often concurrent with biogas production for energy [3–6]. Anaerobic digestion releases organically-bound phosphorus [7,8], leading to dissolved orthophosphate concentrations in anaerobic lagoon effluent that can be in excess of 200 mg P/L [9,10]. Due to the abundance of ammonium (NH_4^+) in anaerobic effluent, phosphorus can be recovered as the mineral struvite ($\text{NH}_4\text{MgPO}_4 \cdot 6\text{H}_2\text{O}(\text{s})$), which can supply both N and P to plants. Because typical anaerobic lagoon effluent is deficient in

magnesium [11], it must be added for struvite precipitation. Magnesium can be added in forms such as MgO(s), Mg(OH)₂(s), MgCl₂·6H₂O(s), seawater, and bittern (solids from evaporated seawater) [12].

Our research focuses on the utilization of agricultural wastes to prepare water treatment materials for phosphorus recovery. Sources of magnesium for phosphorus recovery as struvite include MgO(s) precipitated on high surface area chars prepared from corn cobs and wheat straw, and magnesium silicates prepared using magnesium salts and dissolved silica extracted from rice straw [13]. Other researchers have also utilized Mg-enriched plant chars for phosphorus removal (e.g., [14,15]). Use of agricultural wastes for phosphorus recovery from animal wastewaters is a potentially sustainable approach for phosphorus recycling and reuse.

In concentrated wastewaters and digester effluents, ionic strength and composition could significantly influence the extent of phosphorus removal by precipitation of struvite or other phosphorus minerals. On the one hand, high ionic strength, which tends to stabilize charged species, would tend to increase the solubility of precipitated phosphorus minerals such as struvite, resulting in higher equilibrium concentrations (and poorer removal) of dissolved phosphorus. On the other hand, high ionic strength would also tend to promote the dissolution of Mg²⁺ from Mg(OH)₂(s) or MgO(s), making it more available for reaction with dissolved phosphorus and ammonium. The specific ionic composition of the wastewater could also affect the availability of free Mg²⁺ for struvite formation in several ways. First, carbonate (CO₃²⁻) and bicarbonate (HCO₃²⁻) could exert a magnesium demand to form magnesite (MgCO₃(s)) in high alkalinity wastewaters [16,17]. Alkalinity can be as high as 1890–4938 mg/L as CaCO₃ in the effluent from anaerobic treatment of animal wastewaters [9,18]. Mg²⁺ could also form soluble complexes with CO₃²⁻, HCO₃⁻, Cl⁻, OH⁻, and SO₄²⁻ [19], lowering the concentration of free Mg²⁺ available for struvite formation. For these reasons, concentrations of Mg²⁺ higher than the 1:1 molar ratio of Mg²⁺ to PO₄³⁻ in the mineral struvite are needed for optimum struvite formation [11,20]. Anaerobic digester effluent typically contains an excess of ammonium to phosphate, with reported molar ratios of ammonium to phosphate ranging from four to five [9,21] to more than 20 [22]. In untreated swine wastewaters, ammonium to phosphate molar ratios of more than 60 has been reported [23].

This study aimed to investigate the effect of wastewater ionic strength and composition on the removal of phosphorus by magnesium amended corn cob char and magnesium silicate made from rice straw, and to identify the conditions leading to the greatest phosphorus removal in simple model animal wastewaters. Model animal wastewaters were adjusted to pH 8 or 9 and contained molar ratios of ammonium to phosphate ranging from approximately ten to one hundred. Total magnesium was at least one order of magnitude larger than total phosphorus. Both experimental measurements and chemical equilibrium modeling were performed. Wastewater ionic composition had a strong effect on mineral and aqueous speciation and on the extent of phosphorus removal and recovery.

2. Materials and Methods

2.1. Chemicals and Reagents

Chemicals and their sources were: NaHCO₃ and NaH₂PO₄ (ACS, Fisher Chemical, Fair Lawn, NJ, USA), HCl and HNO₃ (Certified ACS Plus, Fisher Chemical, Fair Lawn, NJ, USA), NaOH (ACS, EMD Chemicals Inc., Gibbstown, NJ, USA), Mg(OH)₂ (95–100.5%, Alfa Aesar, Tewksbury, MA, USA), and NH₄Cl (99.5%, Mallinckrodt Chemicals, Phillipsburg, NJ, USA).

2.2. Preparation of Magnesium Amended Corn Cob Char and Magnesium Amended Rice Straw Ash

Magnesium amended corn cob char (Mg char) was prepared as follows. First, dry corn cobs (Kaytee, Chilton, WI, USA) were ground using an Azadx Model 500# grinder (Amazon.com) to 20–14 mesh (0.84–1.41 mm), washed in deionized (DI) water six times,

soaked in 1 M HNO₃ for 30 min, rinsed with DI water until the rinsate reached pH 6, oven-dried overnight at 60 °C, then sieved to retain the 120–80 mesh fraction. Then, thirty grams of corn cobs treated as described above were mixed with 90 mL water containing 19.3 g Mg(OH)₂ at pH 9.7 for ten hours in capped bottles, oven dried at 100 °C, and then pyrolyzed at 600 °C for six hours in an electric kiln in capped crucibles (to limit oxidation) with the following temperature program: increase temperature by 300 °C per hour to 600 °C, isothermal at 600 °C for six hours, then cool to room temperature naturally. The yield of Mg char from this procedure was 15.53 g. Since 19.3 g Mg(OH)₂ (8.04 g Mg) were added, and the final Mg char weight was 15.53 g, the Mg content in the Mg char was 0.518 g Mg/g or 0.0213 mol Mg/g. Mg char was ground and sieved to retain the 400–120 mesh (38–125 µm) fraction for use in phosphorus uptake experiments.

Magnesium amended rice straw ash (Mg silicate) was prepared as follows. First, rice straw ash was prepared by pyrolysis of ground rice straw (a mixture of *Oryza sativa* and *Tropical japonica*) that was donated by the Dale Bumpers National Rice Research Center, Stuttgart, Arkansas. Details of the procedure were reported previously [13]. Then, one gram of rice straw ash (containing 53% (w/w) silicon [13]) was mixed with 1.03 g Mg(OH)₂, 0.4 g NaOH, and 2.3 L water and stirred in a capped bottle for three days. The pH was 12, which served to dissolve silicon from rice straw ash [24]. The slurry was then settled overnight, filtered in a conical funnel using Grade 1 filter paper (GE Healthcare Whatman, Fisher Scientific, Pittsburgh, PA, USA), rinsed with a small volume (50 mL) of DI water, and the solids oven dried at 60 °C. The solid yield was 0.895 g. Previous XRD analysis showed that this material was mostly amorphous with broad peaks that were consistent with magnesium silicate minerals such as antigorite and enstatite, as well as SiO₂ (quartz) [13]. This material is referred to hereafter as Mg silicate, although its composition is likely heterogeneous. The Mg silicate was then ground and sieved to retain the 400–120 mesh (38–125 µm) fraction for use in phosphorus uptake experiments. Since 1.03 g Mg(OH)₂ (containing 0.429 g Mg) were added to form a final Mg silicate weight of 0.895 g, the Mg content in the Mg silicate was 0.479 g Mg/g or 0.0198 mol Mg/g. Similarly, the Mg silicate also contained 0.0211 mol Si/g. Mg silicate was ground and sieved to retain the 400–120 mesh (38–125 µm) fraction for use in phosphorus uptake experiments.

2.3. Chemical Equilibrium Modeling

Chemical equilibrium modeling was done using MINEQL+ v. 4.6 (Environmental Research Software, Hallowell, ME, USA). Relevant chemical equilibria not already included in the MINEQL+ thermodynamic database (Table A1) were added to MINEQL+ calculations. MINEQL+ component totals and other model settings are given in Tables A2–A4.

2.4. Phosphorus Uptake Experiments

Equilibrium phosphorus removal was measured in a model wastewater containing 0.00221 M NaH₂PO₄ (68.5 mg/L as P), 0.0355 M NaHCO₃ (alkalinity: 0.0355 eq/L, or 1775 mg/L as CaCO₃) [13], and a concentration of NH₄Cl equal to one of the following values: 0.0236 M, 0.059 M, 0.118 M, 0.177 M, or 0.236 M. The concentrations of total orthophosphate, ammonia, and alkalinity in the model wastewater are similar to reported values from actual animal wastewaters [9,18,23]. The concentrations of added NH₄Cl were chosen to yield values of 10.7 to 107 for the molar ratios of total ammonia (i.e., NH₄⁺ and NH₃ and any other complexes or solid phases containing the MINEQL+ component NH₄⁺ (hereafter called [NH₄]_T) to total orthophosphate (hereafter called [PO₄]_T). Solution pH was adjusted to 8 or 9 using NaOH or HCl. The pH of animal wastewaters is typically slightly alkaline, with typical values ranging from 7.5 to 8.3 [9,18,23]. In this study, model wastewaters were adjusted to either pH 8 or 9 to investigate the effect of pH on phosphorus removal as struvite.

A mass of 0.075 g Mg char or Mg silicate was added to 25 mL of model wastewater (3 g/L). The total concentration of Mg in all forms, including free, complexed, and solid (hereafter called [Mg]_T), was 0.064 mol/L in experiments involving Mg char, based on the

Mg content of the char (see above). In the same way, for experiments with Mg silicate, the total concentration (in all forms) of Mg and Si were 0.0593 M and 0.0633 M, respectively. Small amounts of HCl or NaOH were used to adjust the pH and are accounted for in MINEQL+ component totals.

Duplicate samples were equilibrated for 24 h on a Cole-Parmer Ping-Pong TM #51504–00 shaker at 60 excursions per minute, followed by centrifugation at a relative centrifugal force of $3661 \times g$ for 30 min, then filtration using 0.22 μm pore size hydrophilic polyvinylidene fluoride (PVDF) syringe filters (Simsii Inc., Irvine, CA, USA) [13]. Dissolved phosphate in the filtrate was quantified by Method 4500-P. E (Ascorbic acid method) [25] using a Shimadzu UV-1601 spectrophotometer with a wavelength of 880 nm. Procedures to correct for dissolved silica, which produces a colorimetric response similar to phosphate, are described elsewhere [13].

2.5. Measurement of Dissolved $[\text{Mg}]_{\text{T}}$ and $[\text{NH}_4]_{\text{T}}$

Total dissolved ammonia $[\text{NH}_4]_{\text{T}}$ was measured using an ammonia gas sensing electrode (Orion, Thermo Fisher Scientific, Waltham, MA, USA), and dissolved magnesium was measured using a hardness electrode (Cole Parmer, Vernon Hills, IL, USA). Measurements were made on filtered samples after equilibration with phosphate, as described above. Standards of $[\text{NH}_4]_{\text{T}}$ and $[\text{Mg}]_{\text{T}}$ were prepared in the same ionic medium as samples to account for the effects of ionic strength on electrode response.

3. Results and Discussion

3.1. Agreement between Measured Values and MINEQL+ Modeling

Experimentally measured values of dissolved $[\text{Mg}]_{\text{T}}$, $[\text{PO}_4]_{\text{T}}$, and $[\text{NH}_4]_{\text{T}}$ showed good agreement with values calculated by MINEQL+ for experiments with Mg-char at pH 8 (Figure 1). For Mg char at pH 9, however, while measured and calculated concentrations of dissolved $[\text{NH}_4]_{\text{T}}$ and $[\text{Mg}]_{\text{T}}$ were in good agreement (Table A5 (IDs 23–26)), measured dissolved $[\text{PO}_4]_{\text{T}}$ concentrations were significantly lower than values calculated using MINEQL+ (Table A5 (IDs 21–22)). Additionally, for Mg silicate at pH 9, while experimental and calculated values of dissolved $[\text{NH}_4]_{\text{T}}$ were in good agreement (Table A6 (IDs 28–29)), experimental and calculated values of both dissolved $[\text{PO}_4]_{\text{T}}$ and $[\text{Mg}]_{\text{T}}$ differed considerably (Table A6 (IDs 24–27)). These discrepancies could be due to nonequilibrium conditions, effects not considered in the chemical equilibrium model, such as adsorption, or, for dissolved $[\text{PO}_4]_{\text{T}}$, measured values close to or below analytical detection limits (approximately 8×10^{-7} M) at pH 9. Therefore, our discussion below focuses mainly on experiments done with Mg char at pH 8, for which experimental measurements and equilibrium modeling are in good agreement.

3.2. Precipitated Solids

For experiments with Mg char, the molar ratio of $[\text{Mg}]_{\text{T}}:[\text{NH}_4]_{\text{T}}:[\text{PO}_4]_{\text{T}}$ ranged from 29:10.7:1 (for total added NH_4Cl (hereafter called $[\text{NH}_4\text{Cl}]_{\text{T}}$) equal to 0.0236 M) to 29:107:1 (for $[\text{NH}_4\text{Cl}]_{\text{T}} = 0.236$ M). (For experiments with Mg silicate, the ratios were similar and ranged from 27:10.7:1 to 27:107:1.) Thus, neither $[\text{Mg}]_{\text{T}}$ nor $[\text{NH}_4]_{\text{T}}$ limited the formation of struvite under any conditions. Although $[\text{Mg}]_{\text{T}}$ was well in excess of $[\text{PO}_4]_{\text{T}}$ (Tables A2–A4), 52–53% (Figure 2a) of $[\text{Mg}]_{\text{T}}$ was in the form of magnesite ($\text{MgCO}_3(\text{s})$) for Mg char at pH 8. The concentrations of magnesite for Mg char and Mg silicate at pH 9 were similar to those for Mg char at pH 8 (Table 1 (ID 27), Table A5 (ID 27), and Table A6 (ID 30)), indicating that the amount of Mg sequestered in magnesite is a function of total carbonate, which was constant in all three systems. The concentration of Mg sequestered in magnesite for Mg char at pH 8 (3.40×10^{-2} M) was approximately equal to the concentration of added HCO_3^- (3.55×10^{-2} M), meaning that carbonate alkalinity exerted an Mg demand (in moles/L) approximately equal to the alkalinity (in eq/L). (At pH values well above K_{a2} for carbonic acid, i.e., $\text{pH} \gg 10.3$, the Mg demand would be equal to one-half the alkalinity (in eq/L) since one mole of CO_3^{2-} has two equivalents of alkalinity.) Despite the Mg demand of the

carbonate alkalinity, the concentration of dissolved $[\text{Mg}]_{\text{T}}$ (as well as dissolved $[\text{NH}_4]_{\text{T}}$) was still well in excess of $[\text{PO}_4]_{\text{T}}$ (Table 1 (IDs 21–26)) and did not stoichiometrically limit the formation of any magnesium phosphate mineral.

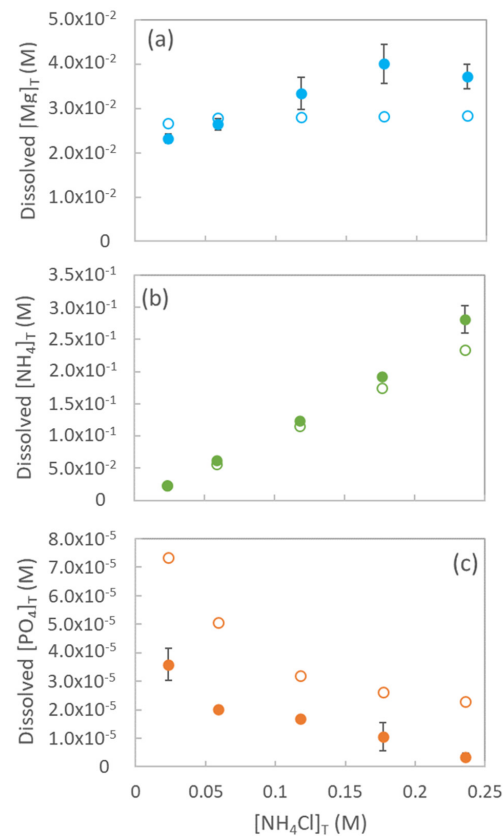


Figure 1. Measured and modeled concentrations of total dissolved (a) $[\text{Mg}]_{\text{T}}$, (b) $[\text{NH}_4]_{\text{T}}$, and (c) $[\text{PO}_4]_{\text{T}}$. Filled symbols are measured values and open symbols are values calculated using MINEQL+. Error bars (for measured values only) are the standard deviations of means of duplicate measurements. In some cases, these error bars are too small to be visible.

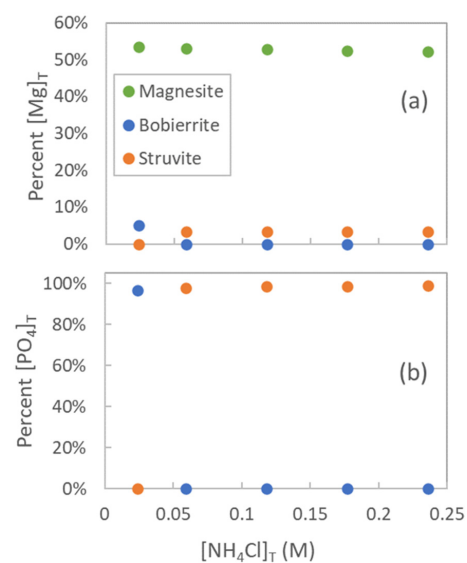


Figure 2. Percent $[\text{Mg}]_{\text{T}}$ and $[\text{PO}_4]_{\text{T}}$ for magnesite, bobierite, and struvite. Symbols are the concentration of each solid (calculated by MINEQL+) divided by (a) $[\text{Mg}]_{\text{T}}$ and (b) $[\text{PO}_4]_{\text{T}}$, then multiplied by 100%.

Table 1. Concentrations of dissolved and solid species for Mg char at pH 8 calculated using MINEQL+. Values for IDs 22, 24, and 26 were measured.

Species ID	Species	Concentration (M)					
		Total added NH ₄ Cl	0.0236	0.059	0.118	0.177	0.236
1	Mg ²⁺		2.42×10^{-2}	2.43×10^{-2}	2.30×10^{-2}	2.19×10^{-2}	2.12×10^{-2}
2	MgOH ⁺		4.37×10^{-6}	4.10×10^{-6}	3.60×10^{-6}	3.28×10^{-6}	3.09×10^{-6}
3	MgHCO ₃ ⁺		9.87×10^{-5}	1.01×10^{-4}	1.04×10^{-4}	1.05×10^{-4}	1.06×10^{-4}
4	MgCO ₃ ⁰		2.88×10^{-5}				
5	MgH ₂ PO ₄ ⁺		6.46×10^{-7}	3.99×10^{-7}	2.05×10^{-7}	1.40×10^{-7}	1.07×10^{-7}
6	MgHPO ₄		4.11×10^{-5}	2.48×10^{-5}	1.25×10^{-5}	8.38×10^{-6}	6.32×10^{-6}
7	MgPO ₄ ⁻		1.62×10^{-7}	9.96×10^{-8}	5.14×10^{-8}	3.51×10^{-8}	2.67×10^{-8}
8	MgCl ⁺		2.21×10^{-3}	3.29×10^{-3}	4.74×10^{-3}	5.93×10^{-3}	6.73×10^{-3}
9	MgNH ₄ OH ²⁺		4.15×10^{-5}	9.81×10^{-5}	1.85×10^{-4}	2.62×10^{-4}	3.36×10^{-4}
10	Mg(NH ₄) ₂ (OH) ₂ ²⁺		4.47×10^{-22}	2.71×10^{-21}	1.19×10^{-20}	2.80×10^{-20}	5.09×10^{-20}
11	H ₃ PO ₄		1.73×10^{-12}	1.14×10^{-12}	6.67×10^{-13}	5.00×10^{-13}	4.04×10^{-13}
12	H ₂ PO ₄ ⁻		1.60×10^{-6}	1.08×10^{-6}	6.49×10^{-7}	4.94×10^{-7}	4.02×10^{-7}
13	HPO ₄ ²⁻		2.26×10^{-5}	1.62×10^{-5}	1.05×10^{-5}	8.40×10^{-6}	7.02×10^{-6}
14	PO ₄ ³⁻		3.60×10^{-9}	2.89×10^{-9}	2.12×10^{-9}	1.83×10^{-9}	1.60×10^{-9}
15	NaHPO ₄ ⁻		3.73×10^{-6}	2.51×10^{-6}	1.53×10^{-6}	1.19×10^{-6}	9.96×10^{-7}
16	NaPO ₄ ²⁻		7.99×10^{-10}	5.75×10^{-10}	3.78×10^{-10}	3.09×10^{-10}	2.65×10^{-10}
17	Na ₂ PO ₄ ⁻		1.62×10^{-10}	1.09×10^{-10}	6.75×10^{-11}	5.39×10^{-11}	4.62×10^{-11}
18	NH ₄ HPO ₄ ⁻		3.51×10^{-6}	5.56×10^{-6}	6.66×10^{-6}	7.55×10^{-6}	8.15×10^{-6}
19	NH ₄ ⁺		2.26×10^{-2}	5.44×10^{-2}	1.11×10^{-1}	1.68×10^{-1}	2.24×10^{-1}
20	NH ₃ (aq)		9.86×10^{-4}	2.33×10^{-3}	4.63×10^{-3}	6.88×10^{-3}	9.13×10^{-3}
21	Dissolved [PO ₄] _T (MINEQL+)		7.34×10^{-5}	5.07×10^{-5}	3.21×10^{-5}	2.62×10^{-5}	2.30×10^{-5}
22	Dissolved [PO ₄] _T (measured)		3.59×10^{-5}	2.02×10^{-5}	1.68×10^{-5}	1.06×10^{-5}	3.46×10^{-6}
23	Dissolved [Mg] _T (MINEQL+)		2.66×10^{-2}	2.78×10^{-2}	2.81×10^{-2}	2.83×10^{-2}	2.84×10^{-2}
24	Dissolved [Mg] _T (measured)		2.32×10^{-2}	2.64×10^{-2}	3.34×10^{-2}	4.01×10^{-2}	3.72×10^{-2}
25	Dissolved [NH ₄ ⁺] _T (MINEQL+)		2.36×10^{-2}	5.68×10^{-2}	1.16×10^{-1}	1.75×10^{-1}	2.34×10^{-1}
26	Dissolved [NH ₄ ⁺] _T (measured)		2.31×10^{-2}	6.19×10^{-2}	1.24×10^{-1}	1.92×10^{-1}	2.81×10^{-1}
27	Magnesite (solid)		3.42×10^{-2}	3.40×10^{-2}	3.38×10^{-2}	3.35×10^{-2}	3.34×10^{-2}
28	Bobierite (solid)		1.07×10^{-3}	0.00	0.00	0.00	0.00
29	Struvite (solid)		0.00	2.16×10^{-3}	2.18×10^{-3}	2.18×10^{-3}	2.19×10^{-3}

According to chemical equilibrium calculations with MINEQL+, the mineral bobierrite (Mg₃(PO₄)₂·8H₂O(s)) formed only at the lowest concentration of [NH₄Cl]_T and removed approximately 97% of [PO₄]_T for Mg char at pH 8 (Figure 2b). Formation of bobierrite, and not struvite, was observed at comparatively low concentrations of NH₄⁺ [26]. According to chemical equilibrium modeling, bobierrite was also the only magnesium phosphate mineral to precipitate at the lowest concentration of [Mg]_T (0.0236 M) at pH 9 for both

Mg char and Mg silicate (Table A5 (ID 28) and Table A6 (ID 31)), for which it removed 99.5% of total added phosphate. Above a $[\text{NH}_4\text{Cl}]_T$ concentration of 0.059 M (a 27:1 molar ratio of $[\text{NH}_4]_T$ to $[\text{PO}_4]_T$), struvite was the only Mg phosphate mineral to form under any conditions (Table 1 (ID 29), Table A5 (ID 29), and Table A6 (ID 32)). For Mg char at pH 8, 98–99% of $[\text{PO}_4]_T$ was in the form of struvite under these conditions (Figure 2b).

3.3. Effect of Solution Composition on Phosphorus Removal

Measured equilibrium phosphorus concentrations were strongly affected by pH, with greater removal (and lower remaining dissolved phosphorus) at pH 9 versus pH 8 (Figure 3). For Mg char at pH 8, measured dissolved phosphorus also decreased with increasing $[\text{NH}_4\text{Cl}]_T$ (Figure 3). This trend was less apparent for experiments with higher $[\text{NH}_4\text{Cl}]_T$ values since many dissolved phosphorus measurements were below detection limits (approximately 8×10^{-7} M) under these conditions (Table A5 (ID 22) and Table A6 (ID 25)), most likely due to the greater abundance of deprotonated PO_4^{3-} and therefore greater driving force for struvite formation. This trend of decreasing soluble $[\text{PO}_4]_T$ with increasing $[\text{NH}_4\text{Cl}]_T$, at least for Mg char at pH 8, cannot be explained by limits on available $[\text{NH}_4]_T$, since $[\text{Mg}]_T$ and $[\text{NH}_4]_T$ were both in excess of $[\text{PO}_4]_T$ under all conditions. Thus, we next considered the possible influence of ionic strength and composition on phosphorus removal.

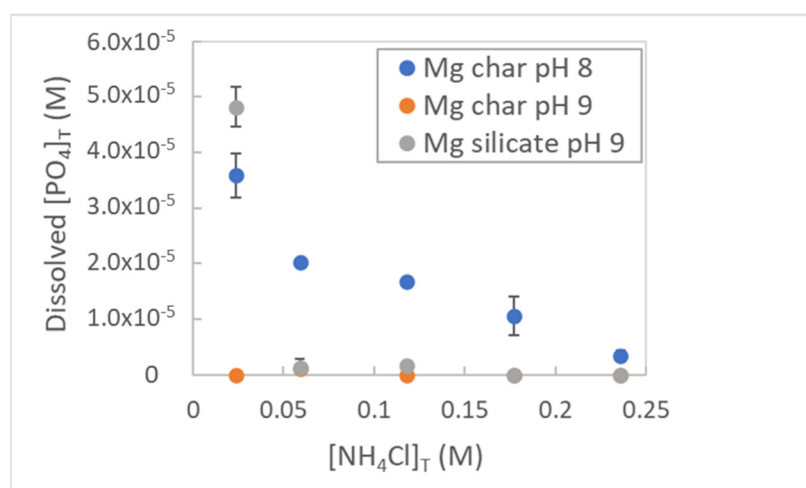


Figure 3. Dissolved $[\text{PO}_4]_T$ (measured) versus $[\text{NH}_4\text{Cl}]_T$. Error bars are standard deviations of the means of duplicate measurements.

We first considered the effect of $[\text{NH}_4\text{Cl}]_T$ on ionic strength. As $[\text{NH}_4\text{Cl}]_T$ increased from 0.0236 M to 0.236 M, the ionic strength increased by a factor of approximately two to three. Calculated values of ionic strength for Mg char at pH 8, based on initial solution recipes (see the Materials and Methods section), were 0.18 M and 0.47 M for the lowest and highest $[\text{NH}_4\text{Cl}]_T$ values, respectively. (For Mg char and Mg silicate at pH 9, the ionic strengths were 0.12 and 0.08 M, respectively, for the lowest $[\text{NH}_4\text{Cl}]_T$ value, and 0.36 and 0.37 M, respectively, for the highest $[\text{NH}_4\text{Cl}]_T$ value.)

The effect of ionic strength on chemical equilibria, and specifically on the solubilities of phosphorus-containing minerals, can be evaluated by calculating conditional (or ionic-strength-dependent) equilibrium constants (cK values) [27]. For bobierrite, struvite, and magnesite, cK values for mineral formation are:

$$\begin{aligned} \text{Bobierrite : } {}^cK &= K \left(\gamma_{\text{Mg}^{+2}} \right)^3 \left(\gamma_{\text{PO}_4^{3-}} \right)^2 \\ \text{Struvite : } {}^cK &= K \gamma_{\text{NH}_4^+} \gamma_{\text{Mg}^{+2}} \gamma_{\text{PO}_4^{3-}} \\ \text{Magnesite : } {}^cK &= K \gamma_{\text{Mg}^{+2}} \gamma_{\text{CO}_3^{2-}} \end{aligned}$$

where K is the equilibrium constant at infinite dilution (i.e., zero ionic strength), and γ values are activity coefficients that depend on ion charge and size. Since activity coefficients for charged species are always less than one, the cK values shown above are always less than the corresponding K values, meaning that the driving force for mineral formation decreases as the ionic strength increases. The effect of ionic strength on cK values, calculated by MINEQL+, for the formation of struvite and magnesite as a function of $[\text{NH}_4\text{Cl}]_T$ for Mg char at pH 8, is illustrated in Figure 4. (cK values for bobierite showed a similar trend, but were much larger (ranging from $10^{21.7}$ to $10^{20.8}$ for the lowest and highest concentrations of $[\text{NH}_4\text{Cl}]_T$, respectively) and were omitted from Figure 4 to better illustrate the other data.)

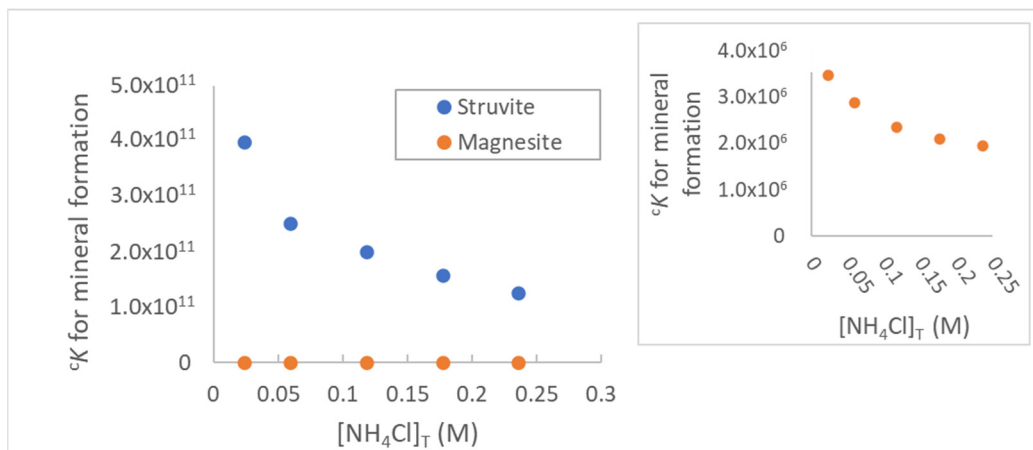


Figure 4. Conditional equilibrium constants (cK values) calculated by MINEQL+ versus $[\text{NH}_4\text{Cl}]_T$.

A comparison of Figures 3 and 4 indicates that $[\text{NH}_4\text{Cl}]_T$ did not affect phosphorus removal solely through its impacts on ionic strength, since the driving force (cK value) for struvite formation decreased with increasing $[\text{NH}_4\text{Cl}]_T$ and increasing ionic strength (Figure 4), while the equilibrium concentration of dissolved phosphorus decreased with increasing $[\text{NH}_4\text{Cl}]_T$ and increasing ionic strength (Figure 3). On the other hand, the cK value for magnesite formation also decreased (Figure 4, inset), and therefore the solubility of magnesite increased with increasing $[\text{NH}_4\text{Cl}]_T$, which could facilitate struvite formation in part by decreasing the amount of Mg sequestered in magnesite. Both measured and MINEQL+ concentrations of total dissolved $[\text{Mg}]_T$ increased with increasing $[\text{NH}_4\text{Cl}]_T$ (Figure 1, Table 1 (IDs 23 and 24)). However, the increase in dissolved $[\text{Mg}]_T$ from the lowest to the highest concentration of $[\text{NH}_4\text{Cl}]_T$ was 1.42×10^{-2} M (measured) and 1.80×10^{-3} M (modeled) (Figure 1, Table 1 (IDs 23 and 24)), which was orders of magnitude greater than the difference in measured dissolved $[\text{PO}_4]_T$ for Mg char at pH 8 between the lowest and highest values of $[\text{NH}_4\text{Cl}]_T$ (3.24×10^{-5} M) (Table 1, ID 22). Thus, the increase in dissolved $[\text{Mg}]_T$ with increasing $[\text{NH}_4\text{Cl}]_T$ cannot by itself explain the decrease in equilibrium dissolved $[\text{PO}_4]_T$ concentration for Mg char at pH 8.

Next, we examined equilibrium speciation of dissolved $[\text{PO}_4]_T$, $[\text{NH}_4]_T$, and $[\text{Mg}]_T$ using MINEQL+ for insights into why aqueous phosphorus concentrations decreased with increasing $[\text{NH}_4\text{Cl}]_T$. Because $[\text{PO}_4]_T$ was present in the lowest molar concentrations relative to $[\text{NH}_4]_T$ and $[\text{Mg}]_T$, it is likely that phosphorus removal by precipitation was driven by dissolved phosphorus speciation, so we examined this further. MINEQL+ output indicates that as $[\text{NH}_4\text{Cl}]_T$ increased from 0.0236 M to 0.236 M for Mg char at pH 8, the concentration of the aqueous species MgCl^+ increased significantly due to the ten-fold increase in the concentration of added Cl^- (the counterion to NH_4^+), as shown in Table 1 (ID 8) and illustrated in Figure 5 (which shows only magnesium phosphate and magnesium chloride complexes for clarity). Trends in the concentration of MgCl^+ were similar for Mg char and Mg silicate at pH 9 (Tables A5 and A6 (ID 8)).

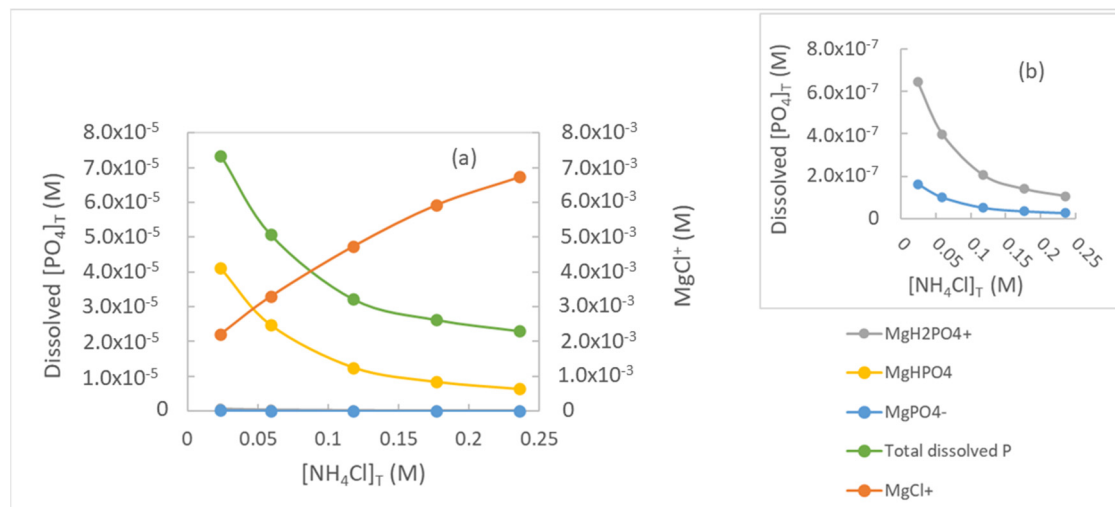


Figure 5. Panel (a): Concentrations of magnesium orthophosphate complexes (left y -axis), along with total dissolved $[\text{PO}_4]_T$ (left y -axis) and MgCl^+ (right y -axis), all calculated with MINEQL+. Panel (b): Inset for panel (a) showing a smaller y -axis scale.

The increase in the proportion of $[\text{Mg}]_T$ in the form of MgCl^+ with increasing $[\text{NH}_4\text{Cl}]_T$ corresponded to a decrease in the proportion of dissolved $[\text{Mg}]_T$ in orthophosphate complexes (Figure 5), essentially freeing orthophosphate to form struvite. Specifically, the decrease in the concentrations of $\text{MgH}_2\text{PO}_4^+$, MgHPO_4 , and MgPO_4^- , (total decrease in concentration: 3.65×10^{-5} M), especially MgHPO_4 (decrease in concentration: 3.48×10^{-5} M), accounts for 72% of the decrease in dissolved $[\text{PO}_4]_T$ (decrease in dissolved $[\text{PO}_4]_T$: 5.04×10^{-5} M) as $[\text{NH}_4\text{Cl}]_T$ increased from 0.0236 M to 0.236 M (Table 1 (IDs 5–7 and 21); Figure 5). Accounting for the complexation of Mg with orthophosphate species (i.e., PO_4^{3-} , HPO_4^{2-} , and H_2PO_4^- , and especially HPO_4^{2-} in the pH range where it is the predominant orthophosphate species (approximately pH 7–12)) is needed to correctly predict the solubility of magnesium phosphate minerals such as struvite [28,29].

While the concentration of the dissolved species $\text{NH}_4\text{HPO}_4^-$ increased by 2.6×10^{-6} M over this same range of $[\text{NH}_4\text{Cl}]_T$ values for Mg char at pH 8, (Table 1 (ID 18)), this concentration increase accounted for only five percent of the decrease in the concentration of total soluble $[\text{PO}_4]_T$ (5.04×10^{-5} M). Thus, the benefit of excess Cl^- in “extracting” Mg^{2+} from magnesium phosphate complexes, making phosphate available to precipitate as struvite, outweighed the drawbacks of NH_4^+ in complexing with dissolved phosphate to form $\text{NH}_4\text{HPO}_4^-$.

Measured concentrations of dissolved $[\text{PO}_4]_T$ were an order of magnitude lower at the highest value of $[\text{NH}_4\text{Cl}]_T$, with an additional 3.24×10^{-5} M $[\text{PO}_4]_T$ (about 1 mg P/L) recovered when $[\text{NH}_4\text{Cl}]_T$ equaled 0.236 M compared to 0.0236 M. This amounted to an additional 1 kg of P that could theoretically be recovered for every million liters of wastewater treated. Using the USDA/IL Dept. of Agriculture price for monoammonium phosphate (MAP, i.e., $\text{NH}_4\text{H}_2\text{PO}_4$) of \$881/ton [30], this additional recovered phosphorus (and nitrogen) as struvite would have a value of \$3.62 per million liters of wastewater treated (assuming a struvite value equal to MAP on a molar basis).

One notable difference between experiments with Mg char and Mg silicate is the presence of dissolved silica in the latter system. MINEQL+ modeling indicates that more than 99.8% of total silica (added as the component orthosilicic acid ($\text{Si}(\text{OH})_4$) in MINEQL+ runs (Table A4)) was present as the mineral quartz (Table A6 (ID 33)). Consequently, dissolved complexes between Mg and orthosilicic acid constituted only a small fraction of dissolved $[\text{Mg}]_T$ (Table A6 (IDs 11–13)). Thus, dissolved silica species in natural waters are unlikely to sequester significant magnesium and thereby affect phosphorus removal via precipitation as bobierrite or struvite in waste treatment systems. This is consistent with

the fact that both Mg char and Mg silica behaved similarly in terms of phosphorus removal at pH 9 (Table A5 (IDs 21–22) and Table A6 (IDs 24–25)).

The formation of significant MgCl^+ in the presence of high concentrations of Cl^- , with Cl^- competing with orthophosphate for free Mg^{2+} , is potentially significant in the application of seawater and seawater bittern for struvite recovery. Bittern is the residue remaining during evaporation of seawater (or other saline natural water) for salt recovery. As evaporation progresses and the seawater becomes more concentrated, salts precipitate in order of decreasing solubility (iron oxides first, then calcite, gypsum, and halite) [31]. Since Mg salts (MgSO_4 and MgCl_2) are comparatively soluble, Mg remains in solution and bittern is enriched in Mg compared to seawater [31], making it an inexpensive source of Mg for struvite formation (e.g., [12]), either through direct addition of bittern to wastewater treatment ponds or through its use in amending water treatment materials such as biochar. Bittern, however, is depleted in Cl^- compared to seawater due to halite (NaCl(s)) removal by precipitation, which could impact Mg speciation and possibly phosphate removal when using bittern as an Mg source for struvite formation in animal wastewaters. Using reported data for seawater and bittern samples from Egypt and India [32], the average molar ratios of Cl to Mg were calculated to be 10 in seawater and 3.1 in bittern. For comparison, the molar ratio of Cl to dissolved Mg for Mg char at pH 8 in this study ranged from 1.0 to 6.3 (for the lowest and highest values of $[\text{NH}_4\text{Cl}]_T$, respectively). Dissolved $[\text{PO}_4]_T$ was significantly lower at the highest versus the lowest value of $[\text{NH}_4\text{Cl}]_T$, for which the Cl:Mg ratio was 6.3 versus 1.0. Specifically, the equilibrium dissolved concentration of $[\text{PO}_4]_T$ decreased by 69% according to chemical equilibrium calculations, and by an order of magnitude based on measurements of dissolved phosphorus, as $[\text{NH}_4\text{Cl}]_T$ increased from 0.0236 M to 0.236 M (Table 1 (IDs 21 and 22)). Thus, the higher Cl:Mg ratio in seawater versus bittern could enhance phosphorus removal and recovery as struvite. At the very least, the influence of dissolved solids in bittern and seawater on phosphorus removal should be evaluated by chemical equilibrium modeling on a case-by-case basis.

4. Conclusions

Magnesium-treated corn cob char (Mg char) effectively removed phosphorus from a model animal wastewater representing anaerobic digester effluent at pH 8, and $[\text{NH}_4\text{Cl}]_T$ had a significant effect on phosphorus recovery and removal. The additional Cl^- at higher $[\text{NH}_4\text{Cl}]_T$ concentrations served to extract Mg from magnesium phosphate complexes, especially MgHPO_4 , freeing orthophosphate to form struvite. Controlling the amount of added Cl^- (and possibly other anions such as SO_4^{2-}) has the potential to increase the efficiency of phosphorus recovery as struvite without raising the wastewater pH.

The high alkalinity in animal wastewaters is likely to exert a significant Mg demand, with the Mg demand (in moles/L) equal to the carbonate alkalinity (in eq/L) at circumneutral and slightly alkaline pH values. In the experiments performed here, using a typical anaerobic digester effluent alkalinity of 0.0355 eq/L (1775 mg/L as CaCO_3), bicarbonate sequestered more than half the added Mg as magnesite, necessitating a significant excess of Mg for phosphorus removal. When using low-cost magnesium sources such as seawater or seawater bittern, the Mg demand due to wastewater alkalinity must be taken into consideration.

Precipitation of bobierite has the potential to significantly lower dissolved phosphorus in wastewaters that have insufficient NH_4^+ for struvite formation (which may occur even when $[\text{NH}_4]_T$ is well in excess of $[\text{PO}_4]_T$, due to the large driving force for bobierite formation). While effective for phosphorus removal, bobierite does not remove $[\text{NH}_4]_T$, which is present in wastewater far in excess of P, and which is an essential plant nutrient.

Author Contributions: Conceptualization, E.C.B., Y.D. and D.A.S.; methodology, E.C.B., Y.D. and D.A.S.; validation, Y.D.; formal analysis, E.C.B.; investigation, Y.D.; resources, E.C.B. and D.A.S.; writing—original draft preparation, E.C.B.; writing—review and editing, Y.D. and D.A.S.; visualization, E.C.B.; supervision, E.C.B. and D.A.S.; project administration, E.C.B.; funding acquisition, E.C.B. and D.A.S. All authors have read and agreed to the published version of the manuscript.

Funding: This work was supported by the Agriculture and Food Research Initiative (AFRI) grant number 2018-67020-27805 from the USDA National Institute of Food and Agriculture.

Institutional Review Board Statement: Not applicable.

Informed Consent Statement: Not applicable.

Data Availability Statement: The data presented in this study are available in the article.

Acknowledgments: The authors thank Anna McClung of the USDA Dale Bumpers National Rice Research Center in Stuttgart, Arkansas, USA for providing the rice straw.

Conflicts of Interest: The authors declare no conflict of interest.

Appendix A.

Appendix A.1. MINEQL+ Input Parameters

Relevant formation reactions between $[\text{PO}_4]_{\text{T}}$, $[\text{Mg}]_{\text{T}}$, and $[\text{NH}_4]_{\text{T}}$, as well as Na^+ , Cl^- , and orthosilicic acid ($\text{Si}(\text{OH})_4$) and its conjugate bases that were not included in the MINEQL+ thermodynamic database (Table A1) were added prior to chemical equilibrium modeling. Equilibrium constants entered into the MINEQL+ database were formation constant for the species of interest (shown on the right-hand side of the equilibria in Table A1) written in terms of MINEQL+ components (shown on the left-hand side of the equilibria in Table A1). To obtain these equilibria and formation constants, equilibria from journal references were rearranged and combined with others in the MINEQL+ database, with corresponding adjustments to the equilibrium constants.

Table A1. Chemical equilibria that were added to the MINEQL+ database.

	Chemical Equilibrium	MINEQL+ Log K Value	Reference
1	$\text{NH}_4^+ + \text{H}^+ + \text{PO}_4^{3-} = \text{NH}_4\text{HPO}_4^-$	13.675	[33]
2	$\text{Na}^+ + \text{H}_2\text{O} - \text{H}^+ = \text{NaOH}^0$	-14.177	[34]
3	$\text{Mg}^{2+} + \text{Cl}^- = \text{MgCl}^+$	0.6	[35]
4	$\text{Na}^+ + \text{PO}_4^{3-} = \text{NaPO}_4^{2-}$	1.43	[35]
5	$2 \text{Na}^+ + \text{PO}_4^{3-} = \text{Na}_2\text{PO}_4^-$	2.59	[35]
6	$\text{Mg}^{2+} + \text{NH}_4^+ - \text{H}^+ = \text{MgNH}_3^{2+}$	-9.004	[35]
7	$\text{Mg}^{2+} + 2 \text{NH}_4^+ - 2 \text{H}^+ = \text{Mg}(\text{NH}_3)_2^{2+}$	-18.288	[35]
8	$\text{Mg}^{+2} + \text{Si}(\text{OH})_4 - \text{H}^+ = \text{MgH}_3\text{SiO}_4^+$	-8.76	[36] *
9	$\text{Mg}^{2+} + 2 \text{Si}(\text{OH})_4 - 2 \text{H}^+ = \text{Mg}(\text{H}_3\text{SiO}_4)_2$	-15.64	[36] *
10	$\text{Mg}^{2+} + \text{Si}(\text{OH})_4 - 2 \text{H}^+ = \text{MgH}_2\text{SiO}_4$	-18.43	[36] *
11	$\text{Mg}^{2+} + \text{NH}_4^+ + \text{PO}_4^{3-} + 6 \text{H}_2\text{O} = \text{MgNH}_4\text{PO}_4 \cdot 6\text{H}_2\text{O}(\text{s})$ (struvite)	13.17	[37]
12	$3 \text{Mg}^{2+} + 2 \text{PO}_4^{3-} + 8 \text{H}_2\text{O} = \text{Mg}_3(\text{PO}_4)_2 \cdot 8\text{H}_2\text{O}(\text{s})$ (bobierrite)	25.2	[26]

Note: * Equilibrium constants reported in this reference were for $I = 0.1 \text{ M}$ and were adjusted to infinite dilution using activity coefficients calculated using the Davies equation.

MINEQL+ component totals are shown in Table A2 (Mg char at pH 8), Table A3 (Mg char at pH 9), and Table A4 (Mg silicate at pH 9). Solution pH was fixed at 8 or 9. Experimental systems were modeled as closed to the atmosphere. All solid phases were MINEQL+ Type V "dissolved solids," meaning they formed if the ion activity product exceeded the solubility constant. Total Cl^- accounts for Cl^- from NH_4Cl and HCl added for pH adjustment. Total Na^+ accounts for Na^+ from NaH_2PO_4 , NaHCO_3 , and NaOH added for pH adjustment. Recipes for solutions are given in the Materials and Methods section.

Table A2. MINEQL+ component totals for Mg char at pH 8.

NH ₄ Cl Added (M)	Component Totals (M)					
	Mg ²⁺	Cl ⁻	Na ⁺	CO ₃ ²⁻	NH ₄ ⁺	PO ₄ ³⁻
0.0236	0.064	0.0686	0.0407	0.0355	0.0236	0.00221
0.059	0.064	0.111	0.0417	0.0355	0.059	0.00221
0.118	0.064	0.186	0.0433	0.0355	0.118	0.00221
0.177	0.064	0.259	0.0450	0.0355	0.177	0.00221
0.236	0.064	0.314	0.0466	0.0355	0.236	0.00221

Table A3. MINEQL+ component totals for Mg char at pH 9.

NH ₄ Cl Added (M)	Component Totals (M)					
	Mg ²⁺	Cl ⁻	Na ⁺	CO ₃ ²⁻	NH ₄ ⁺	PO ₄ ³⁻
0.0236	0.064	0.0236	0.0633	0.0355	0.0236	0.00221
0.059	0.064	0.059	0.0964	0.0355	0.059	0.00221
0.118	0.064	0.118	0.152	0.0355	0.118	0.00221
0.177	0.064	0.177	0.207	0.0355	0.177	0.00221
0.236	0.064	0.236	0.262	0.0355	0.236	0.00221

Table A4. MINEQL+ component totals for Mg silicate at pH 9.

NH ₄ Cl Added (M)	Component Totals (M)						
	Mg ²⁺	Cl ⁻	Na ⁺	CO ₃ ²⁻	NH ₄ ⁺	Si(OH) ₄	PO ₄ ³⁻
0.0236	0.0593	0.0236	0.0464	0.0355	0.0236	0.0633	0.00221
0.059	0.0593	0.059	0.0534	0.0355	0.059	0.0633	0.00221
0.118	0.0593	0.118	0.0650	0.0355	0.118	0.0633	0.00221
0.177	0.0593	0.177	0.0767	0.0355	0.177	0.0633	0.00221
0.236	0.0593	0.236	0.0879	0.0355	0.236	0.0633	0.00221

Appendix A.2. MINEQL+ Output for Mg Char and Mg Silicate at pH 9

The equilibrium concentrations of all species containing the MINEQL+ components Mg²⁺, NH₄⁺, and PO₄³⁻, as well as the measured values of [Mg]_T, [NH₄]_T, and [PO₄]_T, are shown in Table A5 (Mg char at pH 9) and Table A6 (Mg silicate at pH 9).

Table A5. Concentrations of dissolved and solid species for Mg char at pH 9 calculated using MINEQL+. Values in rows 22, 24, and 26 were measured.

Species ID	Species	Concentration (M)					
		Total Added NH ₄ Cl	0.0236	0.059	0.118	0.177	0.236
1	Mg ²⁺		2.42×10^{-2}	2.40×10^{-2}	2.23×10^{-2}	2.09×10^{-2}	1.96×10^{-2}
2	MgOH ⁺		4.51×10^{-5}	4.09×10^{-5}	3.47×10^{-5}	3.09×10^{-5}	2.83×10^{-5}
3	MgHCO ₃ ⁺		9.77×10^{-6}	1.01×10^{-5}	1.04×10^{-5}	1.05×10^{-5}	1.06×10^{-5}
4	MgCO ₃ ⁰		2.88×10^{-5}				
5	MgH ₂ PO ₄ ⁺		6.26×10^{-9}	5.49×10^{-9}	2.83×10^{-9}	1.93×10^{-9}	1.46×10^{-9}
6	MgHPO ₄		4.03×10^{-6}	3.43×10^{-6}	1.71×10^{-6}	1.15×10^{-6}	8.64×10^{-7}
7	MgPO ₄ ⁻		1.57×10^{-7}	1.37×10^{-7}	7.07×10^{-8}	4.82×10^{-8}	3.66×10^{-8}
8	MgCl ⁺		7.91×10^{-4}	1.75×10^{-3}	2.90×10^{-3}	3.82×10^{-3}	4.62×10^{-3}
9	MgNH ₄ OH ²⁺		3.00×10^{-4}	7.01×10^{-4}	1.30×10^{-3}	1.82×10^{-3}	2.28×10^{-3}
10	Mg(NH ₄) ₂ (OH) ₂ ²⁺		2.24×10^{-22}	1.40×10^{-21}	6.32×10^{-21}	1.51×10^{-20}	2.77×10^{-20}

Table A5. Cont.

Species ID	Species	Concentration (M)					
		Total Added NH ₄ Cl	0.0236	0.059	0.118	0.177	0.236
11	H ₃ PO ₄		1.62×10^{-15}	1.57×10^{-15}	9.53×10^{-16}	7.30×10^{-16}	6.06×10^{-16}
12	H ₂ PO ₄ ⁻		1.49×10^{-8}	1.48×10^{-8}	9.29×10^{-9}	7.23×10^{-9}	6.06×10^{-9}
13	HPO ₄ ²⁻		2.03×10^{-6}	2.21×10^{-6}	1.51×10^{-6}	1.24×10^{-6}	1.07×10^{-6}
14	PO ₄ ³⁻		3.07×10^{-9}	3.87×10^{-9}	3.08×10^{-9}	2.75×10^{-9}	2.49×10^{-9}
15	NaHPO ₄ ⁻		5.45×10^{-7}	8.02×10^{-7}	7.67×10^{-7}	8.00×10^{-7}	8.40×10^{-7}
16	NaPO ₄ ²⁻		1.13×10^{-9}	1.82×10^{-9}	1.91×10^{-9}	2.09×10^{-9}	2.26×10^{-9}
17	Na ₂ PO ₄ ⁻		3.73×10^{-10}	8.12×10^{-10}	1.19×10^{-9}	1.66×10^{-9}	2.18×10^{-9}
18	NH ₄ HPO ₄ ⁻		2.36×10^{-7}	5.55×10^{-7}	6.93×10^{-7}	8.06×10^{-7}	8.97×10^{-7}
19	NH ₄ ⁺		1.62×10^{-2}	3.93×10^{-2}	8.08×10^{-2}	1.23×10^{-1}	1.65×10^{-1}
20	NH ₃ (aq)		7.14×10^{-3}	1.68×10^{-2}	3.36×10^{-2}	5.02×10^{-2}	6.68×10^{-2}
21	Dissolved [PO ₄] _T (MINEQL+)		7.02×10^{-6}	7.16×10^{-6}	4.78×10^{-6}	4.06×10^{-6}	3.72×10^{-6}
22	Dissolved [PO ₄] _T (measured)		BDL *	1.09×10^{-6}	BDL	BDL	BDL
23	Dissolved [Mg] _T (MINEQL+)		2.54×10^{-2}	2.65×10^{-2}	2.65×10^{-2}	2.66×10^{-2}	2.66×10^{-2}
24	Dissolved [Mg] _T (measured)		1.40×10^{-2}	1.82×10^{-2}	2.27×10^{-2}	2.72×10^{-2}	2.72×10^{-2}
25	Dissolved [NH ₄ ⁺] _T (MINEQL+)		2.36×10^{-2}	5.68×10^{-2}	1.16×10^{-1}	1.75×10^{-1}	2.34×10^{-1}
26	Dissolved [NH ₄ ⁺] _T (measured)		2.13×10^{-2}	5.75×10^{-2}	1.21×10^{-1}	1.83×10^{-1}	2.44×10^{-1}
27	Magnesite (solid)		3.53×10^{-2}	3.53×10^{-2}	3.53×10^{-2}	3.52×10^{-2}	3.52×10^{-2}
28	Bobierite (solid)		1.10×10^{-3}	0.00	0.00	0.00	0.00
29	Struvite (solid)		0.00	2.20×10^{-3}	2.21×10^{-3}	2.21×10^{-3}	2.21×10^{-3}

Note: * BDL means below detection limits.

Table A6. Concentrations of dissolved and solid species for Mg silicate at pH 9 calculated using MINEQL+. Values for IDs 25, 27, and 29 were measured.

Species ID	Species	Concentration (M)					
		Total Added NH ₄ Cl	0.0236	0.059	0.118	0.177	0.236
1	Mg ²⁺		1.97×10^{-2}	1.96×10^{-2}	1.81×10^{-2}	1.69×10^{-2}	1.59×10^{-2}
2	MgOH ⁺		3.84×10^{-5}	3.53×10^{-5}	2.99×10^{-5}	2.64×10^{-5}	2.38×10^{-5}
3	MgHCO ₃ ⁺		9.62×10^{-6}	9.88×10^{-6}	1.02×10^{-5}	1.04×10^{-5}	1.05×10^{-5}
4	MgCO ₃ ⁰		2.88×10^{-5}				
5	MgH ₂ PO ₄ ⁺		6.64×10^{-9}	5.31×10^{-9}	2.74×10^{-9}	1.87×10^{-9}	1.43×10^{-9}
6	MgHPO ₄		4.33×10^{-6}	3.38×10^{-6}	1.69×10^{-6}	1.13×10^{-6}	8.55×10^{-7}
7	MgPO ₄ ⁻		1.66×10^{-7}	1.33×10^{-7}	6.84×10^{-8}	4.68×10^{-8}	3.58×10^{-8}
8	MgCl ⁺		6.87×10^{-4}	1.54×10^{-3}	2.55×10^{-3}	3.32×10^{-3}	3.95×10^{-3}
9	MgNH ₄ OH ²⁺		2.47×10^{-4}	5.82×10^{-4}	1.07×10^{-3}	1.50×10^{-3}	1.87×10^{-3}
10	Mg(NH ₄) ₂ (OH) ₂ ²⁺		1.63×10^{-6}	9.06×10^{-6}	3.35×10^{-5}	6.94×10^{-5}	1.15×10^{-4}

Table A6. Cont.

Species ID	Species	Concentration (M)				
		Total Added NH ₄ Cl	0.0236	0.059	0.118	0.177
11	MgH ₃ SiO ₄ ⁺	1.66 × 10 ⁻⁶	1.53 × 10 ⁻⁶	1.30 × 10 ⁻⁶	1.14 × 10 ⁻⁶	1.03 × 10 ⁻⁶
12	Mg(H ₃ SiO ₄) ₂	1.72 × 10 ⁻⁸	1.54 × 10 ⁻⁸	1.27 × 10 ⁻⁸	1.10 × 10 ⁻⁸	9.80 × 10 ⁻⁹
13	MgH ₂ SiO ₄	2.80 × 10 ⁻⁷	2.50 × 10 ⁻⁷	2.06 × 10 ⁻⁷	1.78 × 10 ⁻⁷	1.59 × 10 ⁻⁷
14	H ₃ PO ₄	2.02 × 10 ⁻¹⁵	1.76 × 10 ⁻¹⁵	1.07 × 10 ⁻¹⁵	8.31 × 10 ⁻¹⁶	7.03 × 10 ⁻¹⁶
15	H ₂ PO ₄ ⁻	1.83 × 10 ⁻⁸	1.63 × 10 ⁻⁸	1.02 × 10 ⁻⁸	8.11 × 10 ⁻⁹	6.94 × 10 ⁻⁹
16	HPO ₄ ²⁻	2.38 × 10 ⁻⁶	2.31 × 10 ⁻⁶	1.58 × 10 ⁻⁶	1.32 × 10 ⁻⁶	1.18 × 10 ⁻⁶
17	PO ₄ ³⁻	3.33 × 10 ⁻⁹	3.69 × 10 ⁻⁹	2.92 × 10 ⁻⁹	2.70 × 10 ⁻⁹	2.57 × 10 ⁻⁹
18	NaHPO ₄ ⁻	4.97 × 10 ⁻⁷	4.98 × 10 ⁻⁷	3.69 × 10 ⁻⁷	3.38 × 10 ⁻⁷	3.27 × 10 ⁻⁷
19	NaPO ₄ ²⁻	9.87 × 10 ⁻¹⁰	1.07 × 10 ⁻⁹	8.66 × 10 ⁻¹⁰	8.40 × 10 ⁻¹⁰	8.46 × 10 ⁻¹⁰
20	Na ₂ PO ₄ ⁻	2.53 × 10 ⁻¹⁰	2.84 × 10 ⁻¹⁰	2.49 × 10 ⁻¹⁰	2.64 × 10 ⁻¹⁰	2.89 × 10 ⁻¹⁰
21	NH ₄ HPO ₄ ⁻	2.93 × 10 ⁻⁷	6.19 × 10 ⁻⁷	7.76 × 10 ⁻⁷	9.14 × 10 ⁻⁷	1.04 × 10 ⁻⁶
22	NH ₄ ⁺	1.61 × 10 ⁻²	3.91 × 10 ⁻²	8.05 × 10 ⁻²	1.22 × 10 ⁻¹	1.64 × 10 ⁻¹
23	NH ₃ (aq)	7.23 × 10 ⁻³	1.71 × 10 ⁻²	3.41 × 10 ⁻²	5.09 × 10 ⁻²	6.74 × 10 ⁻²
24	Dissolved [PO ₄] _T (MINEQL+)	7.70 × 10 ⁻⁶	6.96 × 10 ⁻⁶	4.50 × 10 ⁻⁶	3.77 × 10 ⁻⁶	3.45 × 10 ⁻⁶
25	Dissolved [PO ₄] _T (measured)	4.82 × 10 ⁻⁵	1.25 × 10 ⁻⁶	1.67 × 10 ⁻⁶	BDL *	BDL
26	Dissolved [Mg] _T (MINEQL+)	2.07 × 10 ⁻²	2.18 × 10 ⁻²	2.18 × 10 ⁻²	2.19 × 10 ⁻²	2.19 × 10 ⁻²
27	Dissolved [Mg] _T (measured)	1.48 × 10 ⁻³	3.90 × 10 ⁻³	6.93 × 10 ⁻³	1.03 × 10 ⁻²	1.19 × 10 ⁻²
28	Dissolved [NH ₄ ⁺] _T (MINEQL+)	2.36 × 10 ⁻²	5.68 × 10 ⁻²	1.16 × 10 ⁻¹	1.75 × 10 ⁻¹	2.34 × 10 ⁻¹
29	Dissolved [NH ₄ ⁺] _T (measured)	2.36 × 10 ⁻²	6.13 × 10 ⁻²	1.17 × 10 ⁻¹	1.80 × 10 ⁻¹	2.45 × 10 ⁻¹
30	Magnesite (solid)	3.53 × 10 ⁻²	3.53 × 10 ⁻²	3.52 × 10 ⁻²	3.52 × 10 ⁻²	3.52 × 10 ⁻²
31	Bobierite (solid)	1.10 × 10 ⁻³	0.00	0.00	0.00	0.00
32	Struvite (solid)	0.00	2.20 × 10 ⁻³	2.21 × 10 ⁻³	2.21 × 10 ⁻³	2.21 × 10 ⁻³
33	Quartz (solid)	6.32 × 10 ⁻²	6.32 × 10 ⁻²	6.32 × 10 ⁻²	6.32 × 10 ⁻²	6.32 × 10 ⁻²

Note: * BDL means below detection limits.

References

1. UNDP. Ocean Hypoxia—'Dead Zones', Issue Brief. May 2013. Available online: http://www.undp.org/content/undp/en/home/librarypage/environment-energy/water_governance/ocean_and_coastalareagovernance/issue-brief--ocean-hypoxia-dead-zones-.html (accessed on 4 October 2016).
2. Dugba, P.N.; Zhang, R.H. Treatment of dairy wastewater with two-stage anaerobic sequencing batch reactor systems—Thermophilic versus mesophilic operations. *Bioresour. Technol.* **1999**, *68*, 225–233. [CrossRef]
3. Midwest Plan Service. *Manure Characteristics. MWPS-18 Section 1*, 2nd ed.; Iowa State University: Ames, IA, USA, 2014.
4. Vanotti, M.B.; Szogi, A.A.; Millner, P.D.; Loughrin, J.H. Development of a second-generation environmentally superior technology for treatment of swine manure in the USA. *Bioresour. Technol.* **2009**, *100*, 5406–5416. [CrossRef]
5. Szogi, A.A.; Vanotti, M.B.; Ro, K.S. Methods for treatment of animal manures to reduce nutrient pollution prior to soil application. *Curr. Pollut. Rep.* **2015**, *1*, 47–56. [CrossRef]
6. Xu, J.L.; Adair, C.W.; Deshusses, M.A. Performance evaluation of a full-scale innovative swine waste-to-energy system. *Bioresour. Technol.* **2016**, *216*, 494–502. [CrossRef]
7. Rittmann, B.E.; Mayer, B.; Westerhoff, P.; Edwards, M. Capturing the lost phosphorus. *Chemosphere* **2011**, *84*, 846–853. [CrossRef]

8. Moller, K.; Muller, T. Effects of anaerobic digestion on digestate nutrient availability and crop growth: A review. *Eng. Life Sci.* **2012**, *12*, 242–257. [[CrossRef](#)]
9. Huchzermeier, M.P.; Tao, W.D. Overcoming Challenges to Struvite Recovery from Anaerobically Digested Dairy Manure. *Water Environ. Res.* **2012**, *84*, 34–41.
10. Foletto, E.L.; Santos, W.R.B.D.; Jahn, S.L.; Bassaco, M.M.; Mazutti, M.A.; Cancelier, A.; Gündel, A. Organic pollutants removal and recovery from animal wastewater by mesoporous struvite precipitation. *Desalination Water Treat.* **2013**, *51*, 2776–2780. [[CrossRef](#)]
11. Beal, L.J.; Burns, R.T.; Stalder, K.J. Effect of anaerobic digestion on struvite production for nutrient removal from swine waste prior to land application. Paper No. 994042. In Proceedings of the 1999 ASAE Annual International Meeting, Toronto, ON, Canada, 18–21 July 1999.
12. Siciliano, A.; Limonti, C.; Curcio, G.M.; Molinari, R. Advances in struvite precipitation technologies for nutrients removal and recovery from aqueous waste and wastewater. *Sustainability* **2020**, *12*, 7538. [[CrossRef](#)]
13. Ding, Y.; Sabatini, D.A.; Butler, E.C. Phosphorus recovery and recycling from model animal wastewaters using materials prepared from rice straw and corn cobs. *Water Sci. Technol.* **2021**, *83*, 1893–1906. [[CrossRef](#)]
14. Yao, Y.; Gao, B.; Chen, J.J.; Yang, L.Y. Engineered Biochar Reclaiming Phosphate from Aqueous Solutions: Mechanisms and Potential Application as a Slow-Release Fertilizer. *Environ. Sci. Technol.* **2013**, *47*, 8700–8708. [[CrossRef](#)]
15. Fang, C.; Zhang, T.; Li, P.; Jiang, R.F.; Wang, Y.C. Application of Magnesium Modified Corn Biochar for Phosphorus Removal and Recovery from Swine Wastewater. *Int. J. Environ. Res. Public Health* **2014**, *11*, 9217–9237. [[CrossRef](#)]
16. Von Breymann, M.T.; Collier, R.; Suess, E. Magnesium adsorption and ion exchange in marine sediments: A multi-component model. *Geochim. Cosmochim. Acta* **1990**, *54*, 3295–3313. [[CrossRef](#)]
17. Song, Y.-H.; Qiu, G.-L.; Yuan, P.; Cai, X.-Y.; Peng, J.-F.; Zeng, P.; Duan, L.; Xiang, L.-C.; Qian, F. Nutrients removal and recovery from anaerobically digested swine wastewater by struvite crystallization without chemical additions. *J. Hazard. Mater.* **2011**, *190*, 140–149. [[CrossRef](#)]
18. Vanotti, M.B.; Szogi, A.A.; Hunt, P.G. Extraction of soluble phosphorus from swine wastewater. *Trans. ASAE* **2003**, *46*, 1665–1674. [[CrossRef](#)]
19. Tao, W.; Fattah, K.P.; Huchzermeier, M.P. Struvite recovery from anaerobically digested dairy manure: A review of application potential and hindrances. *J. Environ. Manag.* **2016**, *169*, 46–57. [[CrossRef](#)]
20. Zeng, L.; Li, X. Nutrient removal from anaerobically digested cattle manure by struvite precipitation. *J. Environ. Eng. Sci.* **2006**, *5*, 285–294. [[CrossRef](#)]
21. Ye, Z.-L.; Chen, S.; Lu, M.; Shi, J.-W.; Lin, L.; Wang, S. Recovering phosphorus as struvite from the digested swine wastewater with bittern as a magnesium source. *Water Sci. Technol.* **2011**, *64*, 334–340.
22. Nelson, N.O.; Mikkelsen, R.L.; Hesterberg, D.L. Struvite precipitation in anaerobic swine lagoon liquid: Effect of pH and Mg:P ratio and determination of rate constant. *Bioresour. Technol.* **2003**, *89*, 229–236. [[CrossRef](#)]
23. Ryu, H.D.; Lee, S.I. Struvite recovery from swine wastewater and its assessment as a fertilizer. *Environ. Eng. Res.* **2016**, *21*, 29–35. [[CrossRef](#)]
24. Adam, F.; Thankappan, R. Oxidation of benzene over bimetallic Cu-Ce incorporated rice husk silica catalysts. *Chem. Eng. J.* **2010**, *160*, 249–258. [[CrossRef](#)]
25. American Public Health Association. *Standard Method 4500-P E: Ascorbic Acid Method*; APHA: Washington, DC, USA, 1992.
26. Warmadewanthi, J.C.L. Recovery of phosphate and ammonium as struvite from semiconductor wastewater. *Sep. Purif. Technol.* **2009**, *64*, 368–373. [[CrossRef](#)]
27. Morel, F.M.M.; Hering, J.G. *Principles and Applications of Aquatic Chemistry*; Wiley: New York, NY, USA, 1993; pp. 80–82.
28. Taylor, A.W.; Frazier, A.W.; Gurney, E.L.; Smith, J.P. Solubility products of di- and trimagnesium phosphates and the dissociation of magnesium phosphate solutions. *Trans. Faraday Soc.* **1963**, *59*, 1585–1589. [[CrossRef](#)]
29. Ohlinger, K.N.; Young, T.M.; Schroeder, E.D. Predicting struvite formation in digestion. *Water Res.* **1998**, *32*, 3607–3614. [[CrossRef](#)]
30. USDA and IL Department of Agriculture. *USDA-IL Dept of Ag Market News Illinois Production Cost Report (Bi-Weekly)*; USDA-IL Dept of Ag Market News Service: Springfield, IL, USA, 2022. Available online: https://www.ams.usda.gov/mnreports/gx_gr210.txt (accessed on 11 June 2022).
31. Abdel-Aal, H.; Zody, K.; Abdelkreem, M. Seawater bittern a precursor for magnesium chloride separation: Discussion and assessment of case studies. *Int. J. Waste Resour.* **2017**, *7*, 1000267.
32. Apriani, M.; Hadi, W.; Masduqi, A. Physicochemical properties of sea water and bittern in Indonesia: Quality improvement and potential resources utilization for marine environmental sustainability. *J. Ecol. Eng.* **2018**, *19*, 1–10. [[CrossRef](#)]
33. Ronteltap, M.; Maurer, M.; Gujer, W. Struvite precipitation thermodynamics in source-separated urine. *Water Res.* **2007**, *41*, 977–984. [[CrossRef](#)]
34. Millero, F.J.; Schreiber, D.R. Use of the ion pairing model to estimate activity coefficients of the ionic components of natural waters. *Am. J. Sci.* **1982**, *282*, 1508–1540. [[CrossRef](#)]
35. Kofina, A.N.; Koutsoukos, P.G. Spontaneous precipitation of struvite from synthetic wastewater solutions. *Cryst. Growth Des.* **2005**, *5*, 489–496.

36. Santschi, P.H.; Schindler, P.W. Complex formation in the ternary systems $\text{Ca}^{\text{II}}\text{-H}_4\text{SiO}_4\text{-H}_2\text{O}$ and $\text{Mg}^{\text{II}}\text{-H}_4\text{SiO}_4\text{-H}_2\text{O}$. *J. Chem. Soc. Dalton Trans.* **1974**, 181–184. [[CrossRef](#)]
37. Hanhoun, M.; Montastruc, L.; Azzaro-Pantel, C.; Biscans, B.; Freche, M.; Pibouleau, L. Temperature impact assessment on struvite solubility product: A thermodynamic modeling approach. *Biochem. Eng. J.* **2011**, *167*, 50–58. [[CrossRef](#)]